

RENF: RETHINKING THE DESIGN SPACE OF NEURAL LONG-TERM TIME SERIES FORECASTERS

Yihang Lu^{1,2}, Xianwei Meng¹, Enhong Chen²

¹Hefei Institutes of Physical Science, Chinese Academy of Sciences, Hefei, China

²University of Science and Technology of China, Hefei, China

lyhsa22@mail.ustc.edu.cn

ABSTRACT

Neural Forecasters (NFs) are a cornerstone of Long-term Time Series Forecasting (LTSF). However, progress has been hampered by an overemphasis on architectural complexity at the expense of fundamental forecasting principles. In this work, we return to first principles to redesign the LTSF paradigm. We begin by introducing a Multiple Neural Forecasting Theorem that provides a theoretical basis for our approach. We propose Boosted Direct Output (BDO), a novel forecasting strategy that synergistically combines the advantages of both Auto-Regressive (AR) and Direct Output (DO). In addition, we stabilize the learning process by smoothly tracking the model’s parameters. Extensive experiments show that these principled improvements enable a simple MLP to achieve state-of-the-art performance, outperforming recent, complex models in nearly all cases, without any specific considerations in the area. Finally, we empirically verify our theorem, establishing a dynamic performance bound and identifying promising directions for future research. The code for review is available at: .

1 INTRODUCTION

The progression of any real-world event is a unique, non-repeatable process, often governed by chaotic dynamics we cannot perfectly measure (Robertson, 1929) or describe. This implies that any observed time series is just one stochastic sample from a complex underlying system. Consequently, a fundamental open question persists: how can we best estimate the long-term future states depending only on a single, observed historical sequence?

Deep Neural Networks (DNNs) have recently received increasing attention in Long-Term Time Series Forecasting (LTSF) (Kim et al., 2025). Their ability to model high-dimensional, non-linear dependencies makes the Neural Forecaster (NF) a promising tool for capturing complex temporal dynamics and implicit dependencies (Laiz et al., 2024). However, the literature reveals several critical problems that should be addressed to unlock the full potential of DNNs in this domain.

One confusing puzzle is that both advanced architectures, like transformer-based (Nie et al., 2023) and simple linear-based models (Zeng et al., 2023), are reported to achieve state-of-the-art performance interchangeably while their complexity varies significantly. This is partly because some datasets prefer parsimonious (Deng et al., 2024) while the others have sufficient volume for complex models to fit. But perhaps a deeper issue is the insufficient exploration of the networks’ intrinsic capabilities. As indicated by (Lu et al., 2025), many NFs contain redundant components and are used selectively depending on the property of the data, resulting in their full potential remaining untapped without extensive tuning or regularizations.

Furthermore, the field’s focus has shifted towards designing specialized modules for properties that are believed to be beneficial for LTSF, such as multi-scale (Wang et al., 2024b) and non-stationary (Liu et al., 2022). However, the progress has become erratic because these architectural additions often yield subtle gains while overlooking fundamental principles. We re-emphasize that progress in this field becomes circuitous when we introduce advanced models merely according to the empirical conclusions from other realms, but overlook the detailed instructions for their full utilization. A primary and more direct path to advancement may lie in fundamentally improving the training stability and generalization capabilities of NFs themselves.

Beyond model architecture, we find that the dominant Direct Output (DO) framework does not make full use of the available supervision. In a standard DO setup, an NF is trained to predict the entire future horizon in a single forward pass, meaning the label information is leveraged only once per optimization step (see Sec.2.3 for the detailed explanation). This encourages the model to finally learn a monolithic representation that maps the entire history to the entire future, without explicitly modeling the sequential dependencies within the forecast itself. We contend that this approach hinders the model from developing a more granular, causal understanding of the future, thereby limiting its full potential.

To address these fundamental shortcomings, this paper proposes a new LTSF framework, derived from first principles, that establishes a reliable and high-performing benchmark model. Our contributions are summarized as follows:

- We propose the Multiple Neural Forecasting Theorem (MNFT) with empirical evaluations, which provides a theoretical foundation and rigorously demonstrates the value of employing multiple Neural Forecasters (NFs) in Long-Term Time Series Forecasting (LTSF).
- We redesign the forecasting architecture by introducing a novel, streamlined forecasting paradigm that synergistically combines the strengths of Direct Output (DO) and Auto Regressive (AR) methods. Furthermore, we apply the Exponential Moving Average (EMA) technique to effectively stabilize the convergence of Neural Forecasters.
- We conduct extensive experiments to demonstrate that a pure MLP-based forecaster, when trained with our paradigm, can significantly outperform recent state-of-the-art models on nearly all standard LTSF benchmarks. These results establish a new and efficient performance baseline for the field.

2 METHOD

In this section, we lay out the theoretical and methodological foundations of our work. We begin by introducing a core theorem that provides the theoretical underpinnings for our approach. To build intuition, we then illustrate our designs using a simple MLP architecture on carefully selected datasets that highlight the key effects of our methods. The comprehensive experimental setup and full results on benchmark datasets are detailed in Sec.3 and the Appendix.

2.1 PRELIMINARIES

Definition 1 (Neural Forecasting Machine). *A Forecasting Machine (FM) is an end-to-end model described by the four-tuple $(t_x, t_y, \theta, \gamma)$, where t_x and t_y denote the input and output lengths. The symbol θ denotes the model’s parameters, and γ denotes the random state encompassing all random factors such as the computational environment and exogenous variables.*

We define the NFM as an FM modeled by neural nets and satisfying that, given an input time series $X \in \mathbb{R}^{t_x}$, an NFM with a determined property tuple $(t_x, t_y, \theta, \gamma)$ yields one and only one series $Y \in \mathbb{R}^{t_y}$ through the operation $Y = \text{NFM}[t_x, t_y, \theta, \gamma](X)$.

Definition 2 (Forecasting Task). *We represent a time series forecasting task with the tuple $(X_h, X_f, \hat{Y}_f, Y_f)$, where X_h, X_f denote the history and future portions of an observed time series. Y_f denotes the expected forecast of X_f , while \hat{Y}_f is an empirical forecast generated by a model such as an NFM. The goal of a forecasting task is to make \hat{Y}_f as close as possible to Y_f with the input X_h .*

2.2 APPROXIMATE THEOREM FOR LTSF

The following theorem provides the theoretical motivation for our work. For simplicity, we just present the proof for the univariate case; however, the theorem can be readily extended to the multivariate setting.

Theorem 1 (Multiple Neural Forecasting Theorem (MNFT)). *Given a NFM $\Phi(t_x, t_y, \theta, \gamma)$ and an observed time series $X_h = (x_1, x_2, \dots, x_n)$ where each element x_t is drawn from a true distribution $p_t(\mu_t, \sigma_t^2)$ with mean μ and standard deviation σ_t . One can generate a series by Φ :*

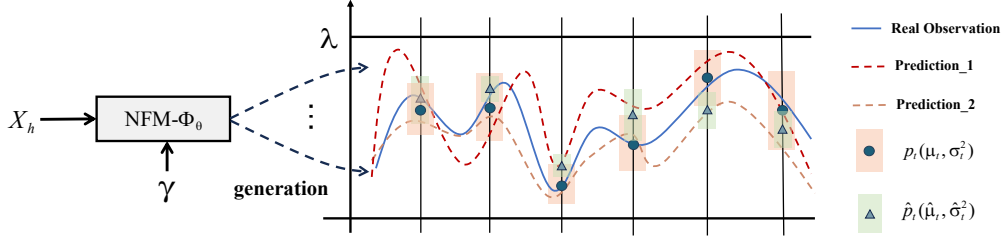


Figure 1: Illustration of the MNFT.

$\hat{Y}_f = (y_1, y_2, \dots, y_T)$ with y_t drawn from the expected forecast distribution $\hat{p}(\hat{\mu}_t, \hat{\sigma}_t^2)$ such that \hat{Y}_f approaches Y_f almost surely, and the error between \hat{Y}_f and X_f is bounded.

Specifically, a trivial but informative upper bound on the l_2 error is given by $T(\lambda + \sqrt{c}(b + \sigma_t))/\sqrt{c}$ under the following mild conditions:

- (A1) The elements in the time series are bounded by a positive real constant λ .
- (A2) The NFM generates candidate series $\{\hat{Y}_f^{(i)}\}_{i=1}^c$ under various θ^i or random states γ^i .
- (A3) Each element in an output series is generated independently.
- (A4) The predictive bias of the NFM is bounded: $\sup_t |\hat{\mu}_t - \mu_t| = b$

We emphasize that condition (A4) distinguishes between the observed real series and the expected true series. This frames the observed data not as the absolute ground truth, but as a single, near-optimal sample from the underlying stochastic process. While it is feasible to theoretically approach the expected forecast, the empirical gap between any observation x_t and the true expectation μ_t is practically irreducible.

The proof of the theorem can be found in Appendix C. To interpret, the shown bound value provides us with some intuitions: for instance, the forecasting error of the NFM naturally grows with the forecast horizon T and the data range λ , because of the expanded solution space.

The most critical insight of the theorem is that an accurate forecast is theoretically achievable even with a rather weak generator, provided a sufficiently large number of candidate outputs is produced. Furthermore, higher-quality historical data and a more powerful NFM (which reduces the estimation error b) both serve to constrain the solution space, leading to better predictions. Inspired by this, we can propose the following conception,

Post combination of multiple forecasts. Given a set of candidate outputs from an NFM, there exist combinatorial methods to synthesize a single, integrated forecast that would be more accurate than any individual candidate. We can represent such a method as an unknown functional g_c that produces the post-combined forecast as:

$$\hat{Y}_{pc} = g_c(\{\hat{Y}_f^{(i)}\}_{i=1}^c) \quad (1)$$

In our experiments, we will empirically show the potential of this combination on real-world datasets. In practice, however, directly creating an optimal combination function without access to future information is a significant challenge. Therefore, designing a framework that can implicitly and effectively leverage these multiple forecasts is one of the key principles guiding our subsequent work.

2.3 NOVEL FORECASTING PARADIGM

The current frameworks in LTSF involve two main strategies: 1-step Auto Regressive (AR(1)) and Direct Output (DO). While AR models perform consistently with recurrent state space models like RNNs (Siami-Namini et al., 2019), they are known to suffer from significant error accumulation in long-horizon forecasting and are empirically evidenced to largely fall behind DO in LTSF (Zhou et al., 2021), making a strong reason for the dominant position of DO in LTSF.

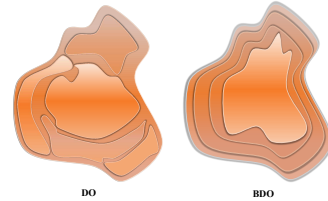


Figure 2: Features of DO and BDO.

However, the shortcomings of the DO approach itself have been largely overlooked. We argue that despite its simplicity, the most significant weakness of DO, particularly when compared to AR, is its lack of inherent causality.

To illustrate this, we conduct a simple experiment in Fig.3: we consecutively split a forecast of length L into m non-overlapped sub-forecasts with length L/m , and each part is predicted by an independent linear head from a shared representation. The final forecast is a concatenation of these segments. Empirically, it turns out that the performance of this multi-headed model is nearly identical to a standard DO model with a single head predicting the full horizon. This result suggests that the NF is unaware of the temporal relationships within the future sequence and makes the prediction without considering the distance/interval between the input history and output future. As a result, it learns to forecast each segment independently, which is fundamentally anti-intuitive.

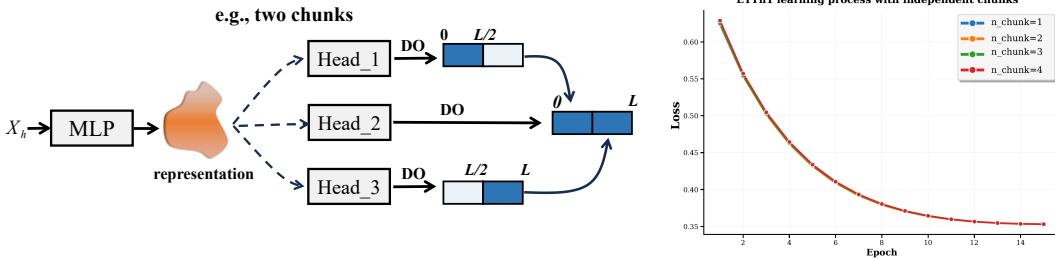


Figure 3: We make the forecast by applying independent heads on several non-overlapped chunks. The right figure shows the learning process in different settings.

According to this observation, we propose a new forecasting paradigm as follows,

Definition 3 (Boost Direct Output (BDO)). *Given a history time series $T_x = \{x_1, x_2, \dots, x_h\}$ (abbr. $T_x\{1 : h\}$) in length h , the NF recursively generates an estimation \hat{T}_y of the future object $T_y = \{y_1, y_2, \dots, y_L\}$ over N -steps. Let $\hat{T}_y\{1 : h_{n-1}\}$ be the forecast at step $n - 1$, then the forecast at step n is:*

$$\hat{T}_y\{1 : h_n\} = NF([T_x, \hat{T}_y\{1 : h_{n-1}\}]), n = 1, 2, \dots, N; \quad (2)$$

where $h_0 = 1$ and $h_N = y_L$. $[\cdot, \cdot]$ indicates the concatenation along the temporal dimension, L is the entire prediction length. In our implementation, we evenly split the forecasting length into n segments for convenience, i.e., in Eq. 2, $h_N = h * N$, where N is a factor of L .

Intuitively, BDO recursively generates forecasts for progressively longer horizons, reusing predictions from previous stages. This incorporates an AR-like causal structure into the forecasting process, while retaining the patch-wise output characteristic of DO that mitigates significant error accumulation. A balance between these two properties can be achieved by properly setting the number of recursive stages, N . Furthermore, since short-term forecasting is generally an easier task than long-term forecasting, BDO effectively creates a learning curriculum. We can reasonably expect this paradigm to outperform both pure AR and pure DO strategies, especially in the challenging LTSF setting.

2.4 MODEL ARCHITECTURE

We construct our NFs using only MLP and linear layers for three primary reasons: 1) As foundational deep learning modules, improvements demonstrated on them are broadly applicable and convincing. 2) Their computational efficiency (low FLOPs) facilitates rapid experimentation and verification. 3) Recent work has shown that simple MLP-based architectures are often sufficient for a wide range of forecasting tasks (Ekambaram et al., 2023).

In principle, we build two NF variants, ReNF- α and ReNF- β , which differ in their degree of non-linearity to better handle datasets of varying complexity. The overall architecture is shown in Fig.4. We stack multiple blocks to adopt the BDO strategy. Each consists of a linear layer for representation projection, followed by an MLP for nonlinear transformation. Each block is also equipped with a dedicated linear head that maps the internal representation back to the data space, steering it to function as a sub-forecaster for horizon $h_j, j = 0, 1, \dots, k$. In the recursive BDO process, the output of each sub-forecaster is concatenated with the original input data to form the new input for the next

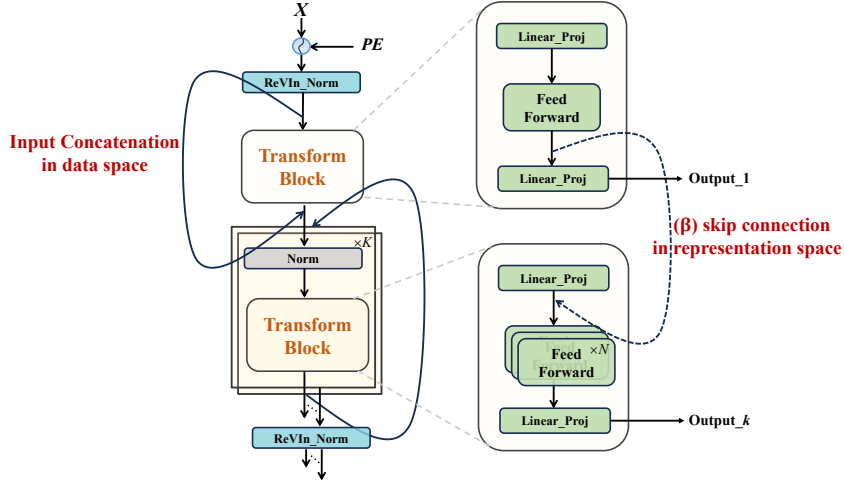


Figure 4: Model Structure of ReNF.

one. To allow for deeper representation flow, the ReNF- β variant also incorporates skip-connections between the representation spaces of consecutive blocks.

We employ RevIN (Kim et al., 2021) as the pre-normalization for the initial input data to reduce the distribution discrepancy between the training and evaluation phases. For consistency, we also apply pre-normalizations to the input of each sub-forecaster. Additionally, we apply dropout before the initial linear projection to prevent the model from being overly dependent on the history observation and the concatenated information in the data space.

The general equation for the transformation process within each sub-forecaster can be written as follows,

$$\text{ReNF_Block}(T) = \text{Proj}(\text{Transform}(\text{Proj}(\text{Norm}(\text{Drop}(T)))))) \quad (3)$$

where T denotes the input series, and all the projections are performed on the temporal dimension.

2.5 LEARNING OBJECTIVE

To train a deterministic NF, we adopt the hybrid loss function as used in (Liu et al., 2025a), which is a convex combination of the Mean Absolute Error (MAE) in both the time and frequency domains. The frequency-domain component has been shown to be effective at reducing spurious autocorrelations in the labels (Wang et al., 2024a).

Our BDO framework uniquely generates multiple outputs of varying lengths, enabling us to apply this loss at each forecasting stage. This hierarchical supervision allows us to fully leverage the label information at multiple scales, encouraging the model to build causally structured and homogeneous representations rather than the disconnected ones typical of standard DO forecasts. In the words of our MNFT, this multi-level supervision provides richer feedback and mutual information from the observed labels, thereby constraining the solution space more effectively.

In the BDO paradigm, the quality of early, short-term forecasts is critical, as errors at these stages may still propagate and degrade the performance of subsequent long-term forecasts. To ensure a stable foundation, we therefore place heavier weights on the losses computed at earlier stages (i.e., for shorter forecast horizons). The complete loss function is expressed as follows:

$$\text{loss} = \sum_{n=1}^N (\gamma/n) * (\alpha * \|\hat{Y}_f^{(n)} - X_f^{(n)}\|_1 + (1 - \alpha) * \|\text{Freq}(\hat{Y}_f^{(n)}) - \text{Freq}(X_f^{(n)})\|_1) \quad (4)$$

where $\|\cdot\|_1$ denotes the l_1 norm, γ and α is predefined coefficients. $\text{Freq}(\cdot)$ represents the discrete fourier transform and $\hat{Y}_f^{(n)}$ denotes the n -th sub-forecast corresponding to the n -th piece of X_f . A more in-depth analysis of this loss function is provided in Appendix D.

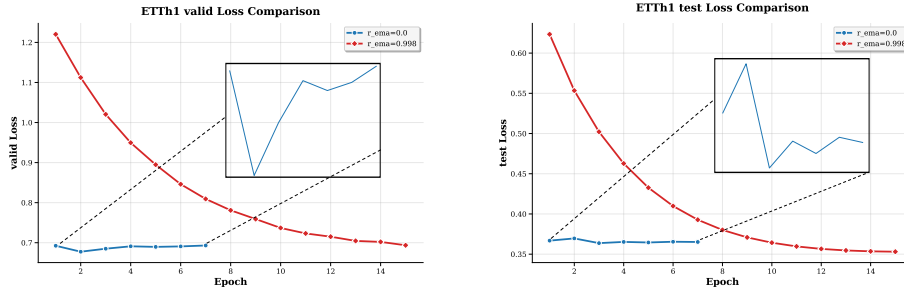


Figure 5: Variation of valid and test loss before and after applying EMA smoothing. The valid loss and test loss are not consistent during the learning process of NFs without smoothing.

2.6 SMOOTHING THE LEARNING FOR TIME SERIES

Notably, training on standard benchmark datasets is often unstable, partly due to sparse or redundant information. The non-stationary nature of real-world time series, combined with chronological data splitting, leads to both internal (batch-to-batch) and external (train/validation/test) distribution mismatches. This causes the optimization path to be heterogeneous, rendering the learning process for NFs ineffective. Specifically, internal data redundancy can cause the model to overfit repeated or spurious patterns (Liu et al., 2025a), harming generalization, while external distribution shift creates inconsistencies across the different phases of training. While normalization techniques like RevIN address the train-test shift, a critical problem remains between validation and testing.

On many datasets, particularly those with smaller volumes, the validation and test losses exhibit significantly different, and at times conflicting, dynamics during training. This issue invalidates the early stopping criterion: learning steps become ineffective, and suboptimal models are saved, preventing a true assessment of a model’s capabilities. This is especially problematic when comparing models of varying complexities, which naturally have different optimization trajectories.

To mitigate these unexpected effects, we propose smoothing the training trajectory by employing a “shadow” model for evaluation. We achieve this efficiently using an Exponential Moving Average (EMA) to track the parameters of the online model, a technique proven effective in self-supervised learning in self-supervised learning (LeCun, 2022) and generative models (Song et al., 2020). Specifically, let θ be the parameters of the online model being trained, and θ' be the parameters of the shadow model. Then the shadow model’s parameters are upgraded as follows at each iteration.

$$\theta'_{\text{new}} = \alpha * \theta'_{\text{prev}} + (1 - \alpha) * \theta_{\text{current}} \tag{5}$$

where α is the EMA decay rate. This shadow model is then used for all evaluations. As shown in Fig. 5, this technique effectively smooths the learning curves and mitigates the inconsistency between validation and test performance. By providing a more stable and reliable training signal, EMA prolongs the effective learning period and enables the model to converge to better local minima, achieving improved generalization.

3 EXPERIMENT

Baselines and Datasets. We compare our model with a suite of recent state-of-the-art methods, including TimeBridge (Liu et al., 2025a), DUET (Qiu et al., 2025), TimeDistill (Ni et al., 2025), Timer-XL (Liu et al., 2025b), iTransformer (Liu et al., 2024), TimeMixer (Wang et al., 2024b), PatchTST (Nie et al., 2023), Crossformer (Zhang & Yan, 2023), and Dlinear (Zeng et al., 2023). We use widely used benchmark datasets in this area, including electricity (ETTh1, ETTh2, ETTm1, ETTm2, Electricity), environment (Weather), energy (Solar-Energy), and transportation (Traffic). Detailed descriptions of these datasets are provided in Appendix B.

Setups. All experiments were conducted on a single NVIDIA 4090 GPU with 24GB of memory, using the Adam optimizer (Kingma & Ba, 2014) and a fixed random seed of 2021 for reproducibility. Results for all baseline models were reproduced using their official source code and optimal configurations. For our model, ReNF, we searched for the optimal learning rate in the range from 0.0001 to 0.005,

the EMA decay rates in the range from 0.99 to 0.999, and the number of layers from 2 to 8. We apply ReNF- α to ETTh1 and ETTh2 datasets, and ReNF- β to others. The look-back window of ReNF is searched over {336, 512, 720} for the best performance. The drop_last bug is corrected following the TFB benchmark (Qiu et al., 2025).

3.1 MAIN RESULT

The results, presented in Table 2, demonstrate a powerful conclusion: without resorting to complex, specialized modules for multi-resolution, periodicity, or cross-variate dependencies, a simple MLP-based model can achieve exceptional performance. **By focusing instead on fundamentally improving the forecasting paradigm and stabilizing the training process**, our MLP model-ReNF sets a new state-of-the-art. Overall, ReNF surpasses all leading 2024 models by a significant margin and outperforms even the most competitive 2025 SOTA methods in almost all cases. This provides strong evidence for the effectiveness of our proposed techniques.

However, we do not claim that existing specialized techniques are redundant. Rather, as discussed in Sec.2.6, many of these architectural designs were evaluated within unstable training frameworks, suggesting that their true effects may need tedious re-evaluation, which may be a promising future work. For instance, on the complex Traffic dataset, while ReNF shows significant improvement over many baselines, it does not surpass the MSE score of the large Transformer-based model, TimeBridge. We compare the model complexity in FLOPs and params between the most competitive models in the Table 1, showing that ReNF reduces 20x the complexity in FLOPs compared to TimeBridge with the Traffic dataset. This suggests that more complex models might still work better on datasets with high non-linearity.

Model		ReNF	TimeBridge	DUET
Weather	Params (MB)	0.200	0.887	4.128
	FLOPs (GB)	0.004	4.262	0.143
ETTh2	Params (MB)	0.393	0.460	4.658
	FLOPs (GB)	0.003	1.604	0.051
Traffic	Param (MB)	21.476	12.431	9.910
	FLOPs (GB)	22.813	479.231	15.575

Table 1: Efficiency comparison of ReNF, TimeBridge, and DUET. All metrics are averaged across the four prediction lengths.

Models	ReNF ours		TimeBridge ((2025a))		DUET (2025)		TimeDistill (2025)		Timer-XL (2025b)		iTransformer (2024)		TimeMixer (2024b)		PatchTST (2023)		Crossformer (2023)		DLinear (2023)	
	MSE	MAE	MSE	MAE	MSE	MAE	MSE	MAE	MSE	MAE	MSE	MAE	MSE	MAE	MSE	MAE	MSE	MAE	MSE	MAE
Weather	0.214	0.247	0.220	0.250	0.219	0.253	0.221	0.269	0.240	0.273	0.232	0.269	0.226	0.264	0.224	0.262	0.232	0.294	0.242	0.293
Electricity	0.145	0.237	0.152	0.247	0.157	0.248	0.157	0.254	0.155	0.246	0.163	0.258	0.185	0.284	0.171	0.271	0.171	0.263	0.167	0.264
Traffic	0.365	0.214	0.357	0.248	0.393	0.256	0.387	0.271	0.374	0.255	0.395	0.279	0.409	0.279	0.397	0.275	0.522	0.282	0.418	0.287
Solar	0.176	0.214	0.183	0.219	0.195	0.214	0.184	0.242	0.198	0.249	0.202	0.262	0.193	0.252	0.200	0.284	0.205	0.233	0.224	0.286
ETTh1	0.331	0.364	0.349	0.380	0.338	0.369	0.348	0.380	0.359	0.382	0.361	0.390	0.356	0.380	0.349	0.381	0.464	0.456	0.356	0.379
ETTh2	0.243	0.301	0.247	0.305	0.248	0.308	0.250	0.312	0.271	0.322	0.269	0.327	0.257	0.318	0.256	0.314	0.501	0.505	0.259	0.325
ETTh1	0.391	0.416	0.401	0.426	0.401	0.420	0.430	0.441	0.409	0.430	0.439	0.448	0.427	0.441	0.419	0.436	0.439	0.461	0.425	0.439
ETTh2	0.327	0.379	0.345	0.386	0.336	0.385	0.345	0.395	0.352	0.402	0.370	0.403	0.349	0.397	0.351	0.395	0.894	0.680	0.470	0.468

Table 2: Results of long-term forecasting of hyperparameter searching. All results are averaged across four different prediction lengths: {96, 192, 336, 720}. The best and second-best results are highlighted in red and blue, respectively. Full results are listed in Appendix E.

3.2 ABLATION STUDY

Effect of EMA. To analyze the impact of EMA, we recorded the evaluation dynamics of ReNF with and without our smoothing technique. The results, shown in Fig. 6, clearly demonstrate EMA’s role. It is notable that we also record the variation of test loss as evidence for the effect of improving the generalization ability.

First, on smaller or less stable datasets like ETTh2, EMA mitigates spurious overfitting and stabilizes the learning curves. This provides a more reliable signal for early stopping and prolongs the effective training period. Second, on large, high-quality datasets such as Electricity, the choice of EMA decay rate can influence performance. By selecting an appropriate rate, the generalization ability of the NF can be substantially enhanced. Full numerical results for all datasets are available in the Appendix.

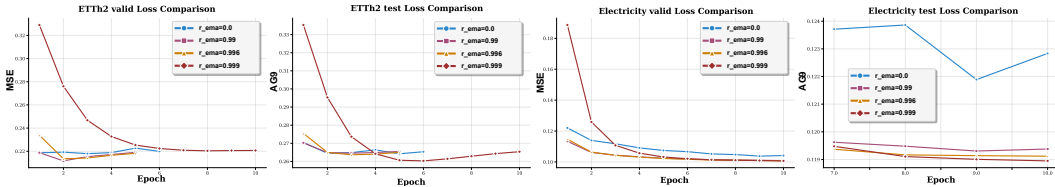


Figure 6: Effect of the EMA smoothing on training and test phase.

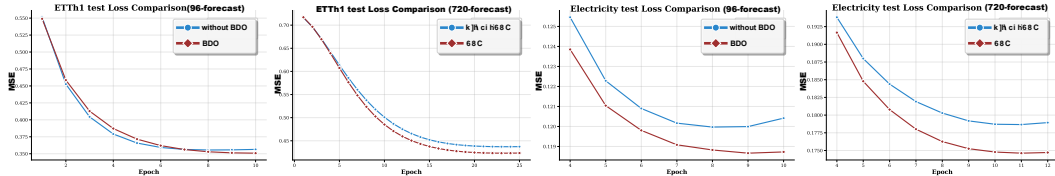


Figure 7: Effect of the BDO forecast.

Effect of BDO. We investigate the effect of the BDO paradigm with the following settings: 1) Keep the depth of ReNF, but disable the recursive input concatenation and apply the loss function only to the final output; 2) Directly change the number of layers/sub-forecasts. By config.1, the BDO reduces to DO with the model structure unchanged. The results, shown in Fig. 7, demonstrate that even on the ETT1 dataset, which has limited data and is difficult to optimize with deep representations, our BDO strategy can still yield superior performance, especially for very long-term forecasts. This finding empirically supports our claim, derived from Theorem 2.2, that leveraging multiple, hierarchically-generated sub-forecasts provides valuable mutual information that enhances the final prediction.

Layer		K=1	K=2	K=3	K=4	K=5	K=6
Weather	MSE	0.311	0.309	0.307	0.307	0.307	0.307
	MAE	0.322	0.320	0.319	0.319	0.319	0.319
ETTh1	MSE	0.411	0.408	0.407	0.406	0.404	0.401
	MAE	0.411	0.409	0.408	0.407	0.407	0.407
Traffic	MSE	0.426	0.415	0.410	0.406	0.403	0.402
	MAE	0.281	0.274	0.272	0.270	0.267	0.267

Table 3: 720-length forecast with varying number of layers (sub-forecasts).

Furthermore, it is shown clearly in Fig. 8(a) that the performance of ReNF with the BDO strategy can consistently improve as K increases. In stark contrast, the performance of the DO model stagnates or degrades with added depth. This difference highlights BDO’s ability to effectively utilize deeper architectures. This meaningful phenomenon suggests that our paradigm may unlock a new, more effective scaling law for LTSF models. Diverse examples are shown in the Table 3 and the Appendix E.

3.3 EMPIRICAL EVALUATION OF THE THEOREM

	Dataset	ETTh1	ETTh2	Weather	Electricity	Solar	Traffic
ReNF	Last Forecast	0.331	0.243	0.391	0.327	0.214	0.145
	Empirical Bound	0.225	0.201	0.270	0.252	0.165	0.100

Table 4: Comparison between the last single forecast and the optimal post-combined forecast of ReNF. The shown metrics are MSE and are averaged across the four prediction lengths.

To empirically evaluate our Multiple Neural Forecasting Theorem (MNFT), we implement the post-combination strategy described in Sec. 2.2. This requires defining a combination function, g_c . While finding an optimal solution without future knowledge is difficult, we can establish a theoretical upper bound on performance. Given the ground truth labels, a trivial yet optimal strategy is to select, at each timestep, the forecast value from among all candidates that has the smallest error. By applying this "oracle" combination, we aim to explore two points: 1) to quantify the potential accuracy improvement achievable through post-combination, thereby establishing a dynamic empirical bound for our forecasting model; and 2) to verify that this empirical bound behaves in a manner consistent with the intuitions of the MNFT 2.2.

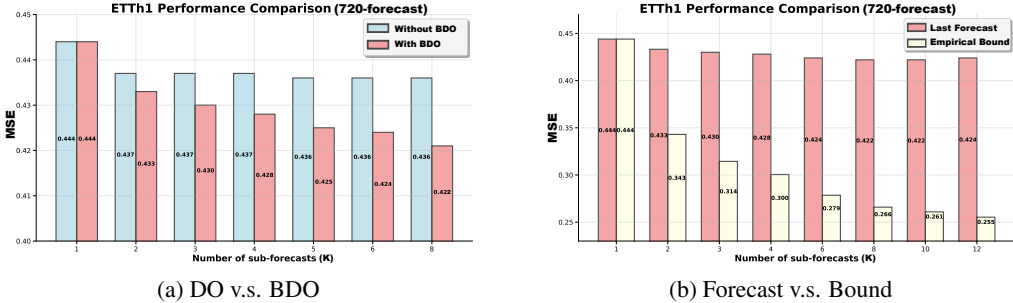


Figure 8: Performance variation with different numbers of sub-forecasts K . (a). Comparison of using DO or BDO. (b). Comparison between the best forecast and the empirical bound of ReNF.

Table 4 presents the performance of this oracle post-combination strategy, revealing a significant gap between the final ReNF forecast and the empirically optimal combination. While this oracle performance is unattainable in practice, the resulting empirical bound is highly informative. On one hand, it indicates that any single forecast is suboptimal and that powerful combinatorial strategies for improving predictions must exist (a promising direction for future work). On the other hand, it shows that we are still far from perfectly leveraging the information contained within the multiple sub-forecasts. This gap is precisely what motivates our BDO paradigm, which is designed to help the neural network implicitly learn a more effective combination function g_c .

Furthermore, Fig. 8(b) shows how this empirical bound varies with the number of sub-forecasts K . The bound consistently decays as K increases, even when the model’s performance saturates. This result aligns perfectly with the core insight from MNFT: the theoretical performance limit improves as the number of candidate forecasts grows.

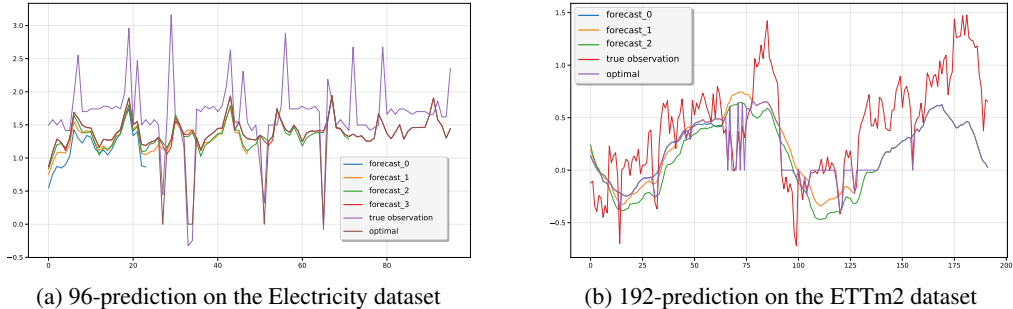


Figure 9: Visualization of forecasting results of ReNF. The figure shows multiple outputs of ReNF in different layers, along with the result of applying optimal post-combination.

In a nutshell, our evaluation of the MNFT clarifies two primary roles for Neural Networks in this domain. First, NNs should be leveraged to learn a powerful post-combination function over multiple candidate forecasts. Second, more powerful base forecasters must be developed to better approximate the true data-generating distribution, directly reducing the predictive bias b as identified in our theorem 2.2.

4 CONCLUSION

We propose a fundamental theorem to support the mechanism of multiple forecasts. Based on this theorem, we introduce a novel paradigm that combines the advantages of current forecasting methods, enabling more accurate predictions in a hierarchical representation space. To remedy training instability, we leverage EMA to smooth the learning process of neural forecasters. Our empirical results show that with these techniques, a simple MLP can outperform recent SOTA models with significantly less complexity. The value of our theorem is also evaluated and confirmed by experimental results, clearly identifying the role of the Neural Network in building the Long-Term Time Series forecasters.

5 REPRODUCIBILITY STATEMENT

We have put a lot of effort into ensuring the reproducibility of this work, including the code in the anonymous repository , a complete data description in the Appendix B, and clear explanations of the assumptions and proof of the proposed theorem in the Appendix C.

REFERENCES

- John M Bates and Clive WJ Granger. The combination of forecasts. *Journal of the operational research society*, 20(4):451–468, 1969.
- Leo Breiman. Bagging predictors. *Machine learning*, 24(2):123–140, 1996.
- Tianqi Chen and Carlos Guestrin. Xgboost: A scalable tree boosting system. In *Proceedings of the 22nd acm sigkdd international conference on knowledge discovery and data mining*, pp. 785–794, 2016.
- Robert T Clemen. Combining forecasts: A review and annotated bibliography. *International journal of forecasting*, 5(4):559–583, 1989.
- Adrien Cortés, Rémi Rehm, and Victor Letzelter. Winner-takes-all for multivariate probabilistic time series forecasting. *arXiv preprint arXiv:2506.05515*, 2025.
- Jinliang Deng, Feiyang Ye, Du Yin, Xuan Song, Ivor Tsang, and Hui Xiong. Parsimony or capability? decomposition delivers both in long-term time series forecasting. *Advances in Neural Information Processing Systems*, 37:66687–66712, 2024.
- Vijay Ekambaram, Arindam Jati, Nam Nguyen, Phanwadee Sinthong, and Jayant Kalagnanam. Tsmixer: Lightweight mlp-mixer model for multivariate time series forecasting. In *Proceedings of the 29th ACM SIGKDD conference on knowledge discovery and data mining*, pp. 459–469, 2023.
- Jongseon Kim, Hyungjoon Kim, HyunGi Kim, Dongjun Lee, and Sungroh Yoon. A comprehensive survey of deep learning for time series forecasting: architectural diversity and open challenges. *Artificial Intelligence Review*, 58(7):1–95, 2025.
- Taesung Kim, Jinhee Kim, Yunwon Tae, Cheonbok Park, Jang-Ho Choi, and Jaegul Choo. Reversible instance normalization for accurate time-series forecasting against distribution shift. In *International conference on learning representations*, 2021.
- Diederik P Kingma and Jimmy Ba. Adam: A method for stochastic optimization. *arXiv preprint arXiv:1412.6980*, 2014.
- Dilfira Kudrat, Zongxia Xie, Yanru Sun, Tianyu Jia, and Qinghua Hu. Patch-wise structural loss for time series forecasting. *arXiv preprint arXiv:2503.00877*, 2025.
- Rodrigo González Laiz, Tobias Schmidt, and Steffen Schneider. Self-supervised contrastive learning performs non-linear system identification. *arXiv preprint arXiv:2410.14673*, 2024.
- Yann LeCun. A path towards autonomous machine intelligence version 0.9. 2, 2022-06-27. *Open Review*, 62(1):1–62, 2022.
- Shengsheng Lin, Haojun Chen, Haijie Wu, Chunyun Qiu, and Weiwei Lin. Temporal query network for efficient multivariate time series forecasting. *arXiv preprint arXiv:2505.12917*, 2025.
- Peiyuan Liu, Beiliang Wu, Yifan Hu, Naiqi Li, Tao Dai, Jigang Bao, and Shu-tao Xia. Timebridge: Non-stationarity matters for long-term time series forecasting. *arXiv preprint arXiv:2410.04442*, 2025a.
- Yong Liu, Haixu Wu, Jianmin Wang, and Mingsheng Long. Non-stationary transformers: Exploring the stationarity in time series forecasting. *Advances in neural information processing systems*, 35: 9881–9893, 2022.

- Yong Liu, Tengge Hu, Haoran Zhang, Haixu Wu, Shiyu Wang, Lintao Ma, and Mingsheng Long. itransformer: Inverted transformers are effective for time series forecasting. *arXiv preprint arXiv:2310.06625*, 2024.
- Yong Liu, Guo Qin, Xiangdong Huang, Jianmin Wang, and Mingsheng Long. Timer-xl: Long-context transformers for unified time series forecasting. *arXiv preprint arXiv:2410.04803*, 2025b.
- Yihang Lu, Yangyang Xu, Qitao Qin, and Xianwei Meng. Timecapsule: Solving the jigsaw puzzle of long-term time series forecasting with compressed predictive representations. In *Proceedings of the 31st ACM SIGKDD Conference on Knowledge Discovery and Data Mining V. 2*, pp. 1987–1998, 2025.
- Dhruv D Modi and Rong Pan. Enhancing transformer-based foundation models for time series forecasting via bagging, boosting and statistical ensembles. *arXiv preprint arXiv:2508.16641*, 2025.
- Mehryar Mohri, Afshin Rostamizadeh, and Ameet Talwalkar. *Foundations of machine learning*. MIT press, 2018.
- Hanh H Nguyen and Christine W Chan. Multiple neural networks for a long term time series forecast. *Neural Computing & Applications*, 13(1):90–98, 2004.
- Juntong Ni, Zewen Liu, Shiyu Wang, Ming Jin, and Wei Jin. Timedistill: Efficient long-term time series forecasting with mlp via cross-architecture distillation. *arXiv preprint arXiv:2502.15016*, 2025.
- Yuqi Nie, Nam H Nguyen, Phanwadee Sinthong, and Jayant Kalagnanam. A time series is worth 64 words: Long-term forecasting with transformers. *arXiv preprint arXiv:2211.14730*, 2023.
- Boris N Oreshkin, Dmitri Carpov, Nicolas Chapados, and Yoshua Bengio. N-beats: Neural basis expansion analysis for interpretable time series forecasting. *arXiv preprint arXiv:1905.10437*, 2019.
- Xiangfei Qiu, Xingjian Wu, Yan Lin, Chenjuan Guo, Jilin Hu, and Bin Yang. Duet: Dual clustering enhanced multivariate time series forecasting. In *Proceedings of the 31st ACM SIGKDD Conference on Knowledge Discovery and Data Mining V. 1*, pp. 1185–1196, 2025.
- Howard Percy Robertson. The uncertainty principle. *Physical Review*, 34(1):163, 1929.
- Sima Siami-Namini, Neda Tavakoli, and Akbar Siami Namin. The performance of lstm and bilstm in forecasting time series. In *2019 IEEE International conference on big data (Big Data)*, pp. 3285–3292. IEEE, 2019.
- Yang Song, Jascha Sohl-Dickstein, Diederik P Kingma, Abhishek Kumar, Stefano Ermon, and Ben Poole. Score-based generative modeling through stochastic differential equations. *arXiv preprint arXiv:2011.13456*, 2020.
- Hao Wang, Licheng Pan, Zhichao Chen, Degui Yang, Sen Zhang, Yifei Yang, Xinggao Liu, Haoxuan Li, and Dacheng Tao. Fredf: Learning to forecast in the frequency domain. *arXiv preprint arXiv:2402.02399*, 2024a.
- Shiyu Wang, Haixu Wu, Xiaoming Shi, Tengge Hu, Huakun Luo, Lintao Ma, James Y Zhang, and Jun Zhou. Timemixer: Decomposable multiscale mixing for time series forecasting. *arXiv preprint arXiv:2405.14616*, 2024b.
- Wang Xue, Tian Zhou, Qingsong Wen, Jinyang Gao, Bolin Ding, and Rong Jin. Card: Channel aligned robust blend transformer for time series forecasting. *arXiv preprint arXiv:2305.12095*, 2023.
- Wang Xue, Tian Zhou, Qingsong Wen, Jinyang Gao, Bolin Ding, and Rong Jin. Card: Channel aligned robust blend transformer for time series forecasting. *arXiv preprint arXiv:2305.12095*, 2024.

Wenzhen Yue, Yong Liu, Haoxuan Li, Hao Wang, Xianghua Ying, Ruohao Guo, Bowei Xing, and Ji Shi. Olinear: A linear model for time series forecasting in orthogonally transformed domain. *arXiv preprint arXiv:2505.08550*, 2025.

Ailing Zeng, Muxi Chen, Lei Zhang, and Qiang Xu. Are transformers effective for time series forecasting? In *Proceedings of the AAAI conference on artificial intelligence*, volume 37, pp. 11121–11128, 2023.

G Peter Zhang. Time series forecasting using a hybrid arima and neural network model. *Neurocomputing*, 50:159–175, 2003.

Yunhao Zhang and Junchi Yan. Crossformer: Transformer utilizing cross-dimension dependency for multivariate time series forecasting. In *The eleventh international conference on learning representations*, 2023.

Haoyi Zhou, Shanghang Zhang, Jieqi Peng, Shuai Zhang, Jianxin Li, Hui Xiong, and Wancai Zhang. Informer: Beyond efficient transformer for long sequence time-series forecasting. In *Proceedings of the AAAI conference on artificial intelligence*, volume 35, pp. 11106–11115, 2021.

Supplementary Material

A RELATED WORK

We note that ReNF is not the first work to address LTSF using multiple short-term forecasts. A pioneering and highly relevant study by (Nguyen & Chan, 2004) proposed a machine called MNN, which generates long-term forecasts using multiple neural networks, each responsible for a specific interval of the output. The essential distinction between MNN and our approach is that we generate sub-forecasts recursively, with the explicit goal of injecting causality into the DO strategy. In contrast, each sub-network in MNN functions as a standalone AR(1) model. This difference stems from our distinct motivation: whereas MNN was designed primarily to mitigate the error accumulation of one-step-ahead NN models, our work begins with a foundational forecasting theorem. Based on this theorem, we leverage modern deep learning techniques to effectively utilize multiple sub-forecasts, achieving strong empirical results on a wide range of real-world datasets, which constitutes one of our main contributions.

A recently proposed work using the multiple-choice learning paradigm (Cortés et al., 2025) is also relevant, as it demonstrates an ability to handle the diverse and multi-modal nature of the future from a probabilistic perspective. Furthermore, the characterization of TimeMCL as a conditional stationary quantizer for time series may offer additional theoretical support and interpretations for our framework.

Our work also connects to classic ensemble methods in machine learning (Mohri et al., 2018). For instance, the recursive workflow of ReNF is analogous to gradient-boosted regression models (Chen & Guestrin, 2016), which construct a strong predictor from multiple weak ones. Additionally, the collaborative training can be viewed as a form of bagging (Breiman, 1996), which effectively resamples the data to train diverse forecasters. In this context, an even more recent study (Modi & Pan, 2025) re-certified the benefits of such ensemble methods for enhancing Transformer-based NFs, providing further empirical support for the direction of our research.

Forecast Combinations. Forecast combination is a classic technique for improving forecast accuracy and robustness by leveraging the diverse strengths of multiple models (Clemen, 1989). In this work, we extend this concept (Bates & Granger, 1969) to the domain of deep learning for long-term time series forecasting. Rather than combining distinct, parallel forecasters into a hybrid model (Zhang, 2003), our framework achieves this goal efficiently within a single neural network. By recursively stacking sub-forecasts, similar in spirit to N-BEATS (Oreshkin et al., 2019), we ensure that the representation learning is both deep and diverse, allowing the LSTF task to benefit from the full power of modern machine learning.

B DETAILS OF DATASETS

Dataset	Dim	Prediction Length	Split	Frequency	domain
ETTh1, ETTh2	7	96, 192, 336, 720	(6, 2, 2)	Hourly	Electricity
ETTm1, ETTm2	7	96, 192, 336, 720	(6, 2, 2)	15min	Electricity
Weather	21	96, 192, 336, 720	(7, 1, 2)	10min	Environment
Electricity	321	96, 192, 336, 720	(7, 1, 2)	Hourly	Electricity
Traffic	862	96, 192, 336, 720	(7, 1, 2)	Hourly	Transportation
Solar	137	96, 192, 336, 720	(6, 2, 2)	10min	Energy

Table 5: Descriptions of multivariate time series datasets used in this research. The dim column represents the number of variates, and the split column specifies the train-validate-test splitting ratio for each dataset.

The ETTh1, ETTh2, ETTm1, and ETTm2 datasets record the temperature of electricity transformers every hour and every 15 minutes. The Weather dataset contains 21 weather information, measured every 10 minutes in Germany. The Electricity dataset records the amount of electricity used by 321 customers every hour. The ILI dataset records how many patients there are and how many have influenza-like illnesses (ILI) every week. The Solar dataset records how much electricity is produced by solar power stations every 10 minutes, from 137 solar power stations, in 2006. The Traffic dataset records how busy the roads are in San Francisco, every hour, from 862 sensors on the freeway. We also include the PEMS04 dataset, which contains information about the traffic network in California, collected every 5 minutes. This is often used to make predictions about the movement of traffic.

C PROOF OF THE APPROXIMATE THEOREM

We restate and emphasize the preconditions of our proof:

- (A1) The elements in the time series are bounded by a positive real constant λ . (We also assume the observed series is normal and noiseless for simplicity.)
- (A2) The NFM generates c candidate series $\{\hat{Y}_f^{(i)}\}_{i=1}^c$ under various $\theta^{(i)}$ or random states $\gamma^{(i)}$.
- (A3) Each element in an output series is generated independently. (This can be satisfied in the DO framework as discussed in Sec.2.3.)
- (A4) The predictive bias of the NFM is bounded: $\sup_t |\hat{\mu}_t - \mu_t| = b$

Proof. First, we derive the expected bound for each independent element $y_t^{(i)}$ in any candidate forecast $\hat{Y}_f^{(i)} = \{y_1^{(i)}, y^{(i)}, \dots, y_c^{(i)}\}$.

Since $y_t^{(i)} \sim \hat{p}(\hat{\mu}_t, \hat{\sigma}_t^2)$, we know from the (A2) that $\{y_t^{(i)}\}_{i=1}^c$ are i.i.d. samples from the same distribution with $\mathbb{E}(y_t^{(i)}) = \hat{\mu}_t$. Thus, according to the law of large numbers, the statistical average of $\{y_t^{(i)}\}_{i=1}^c$ converges to the expectation μ_t almost surely as $c \rightarrow \infty$.

In particular, we have

$$\mathbb{E}|\hat{\mu}_t - \frac{1}{c} \sum_{i=1}^c y_t^{(i)}|^2 = \mathbb{E}|\frac{1}{c} \sum_{i=1}^c (y_t^{(i)} - \hat{\mu}_t) + \hat{\mu}_t - \mu_t|^2 \quad (6)$$

$$= \frac{1}{c^2} \mathbb{E}|\sum_{i=1}^c (y_t^{(i)} - \hat{\mu}_t)|^2 \quad (7)$$

$$= \frac{1}{c^2} \sum_{i=1}^c \mathbb{E}|y_t^{(i)} - \hat{\mu}_t|^2. \quad (8)$$

The last identity holds because $\{y_t^{(i)}\}_{i=1}^c$ are independent, i.e., $\mathbb{E}[(y_t^{(i)} - \hat{\mu}_t)(y_t^{(j)} - \hat{\mu}_t)] = \mathbb{E}(y_t^{(i)} - \hat{\mu}_t) \cdot \mathbb{E}(y_t^{(j)} - \hat{\mu}_t) = 0, i \neq j$.

Then, we can bound this term by showing

$$\mathbb{E}|y_t^{(i)} - \hat{\mu}_t|^2 = \mathbb{E}|y_t^{(i)} - \mathbb{E}[y_t^{(i)}]|^2 \quad (9)$$

$$= \mathbb{E}|y_t^{(i)}|^2 - |\mathbb{E}[y_t^{(i)}]|^2 \text{ (variance identity)} \quad (10)$$

$$\leq \mathbb{E}[(y_t^{(i)})^2] \quad (11)$$

$$\leq \sup_{i,t} \{(y_t^{(i)})^2\} = \lambda^2. \text{ (A1)} \quad (12)$$

Therefore, we have shown that

$$\mathbb{E}|\hat{\mu}_t - \frac{1}{c} \sum_{i=1}^c y_t^{(i)}|^2 \leq \frac{\lambda^2}{c}. \quad (13)$$

for any i ; and in particular, there must exist a set of $\{\tilde{y}_t^{(i)}\}_{i=1}^c$ satisfying

$$|\hat{\mu}_t - \frac{1}{c} \sum_{i=1}^c \tilde{y}_t^{(i)}| \leq \frac{\lambda}{\sqrt{c}}. \quad (14)$$

Fixing the set $\{\tilde{y}_t^{(i)}\}_{i=1}^c$, it remains to estimate the distance between the forecast by the NFM Φ and the expected forecast Y_f , and the true observation X_f , respectively.

Since it is trivial to get

$$|\mu_t - \frac{1}{c} \sum_{i=1}^c \tilde{y}_t^{(i)}| \leq |\hat{\mu}_t - \frac{1}{c} \sum_{i=1}^c \tilde{y}_t^{(i)}| + |\hat{\mu}_t - \mu_t| \leq |\hat{\mu}_t - \frac{1}{c} \sum_{i=1}^c \tilde{y}_t^{(i)}| + b. \quad (A4) \quad (15)$$

We have

$$|x_t - \frac{1}{c} \sum_{i=1}^c \tilde{y}_t^{(i)}| \leq |\mu_t - \frac{1}{c} \sum_{i=1}^c \tilde{y}_t^{(i)}| + |x_t - \mu_t| \leq |\hat{\mu}_t - \frac{1}{c} \sum_{i=1}^c \tilde{y}_t^{(i)}| + b + \sigma. \quad (A1) \quad (16)$$

Thus, we can derive the expected upper bound as

$$\sum_{t=1}^T |x_t - \frac{1}{c} \sum_{i=1}^c \tilde{y}_t^{(i)}| \leq T \cdot (\frac{\lambda}{c} + b + \sigma) = \frac{T(\lambda + \sqrt{c}(b + \sigma))}{\sqrt{c}}. \quad (A3) \quad (17)$$

This completes the proof.

Note that the above proof is based on a univariate time series; however, it is easy to extend the result to the multivariate case using a similar process in a certain normed vector space.

D IMPLICIT STRUCTURAL LOSS

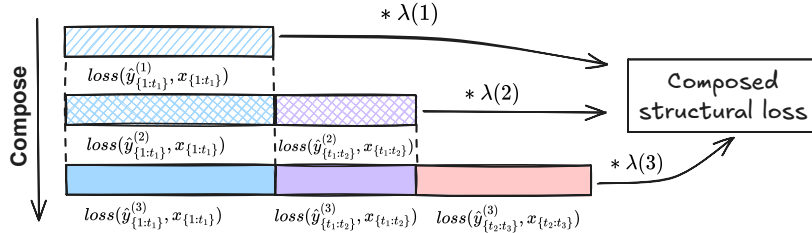


Figure 10: Illustration of the implicit structural loss of BDO, we exemplify it in the NF consisting of three sub-forecasters.

An interesting property of the BDO paradigm is the implicit structural loss it induces. This connects our work to recent research on explicit loss engineering, such as positional weighting (Xue et al., 2023) and patch-wise structural losses (Kudrat et al., 2025). We posit that the BDO learning objective, formed by the weighted sum of losses from hierarchical sub-forecasts, inherently functions as a complex structural loss. This seemingly implicit loss can be seen as the generalized version of the above two.

To formalize this property, we first simplify the loss function from Eq.4 as:

$$Loss = \sum_{n=1}^N \lambda(n) * f(\hat{Y}_f^{(n)}, X_f^{(n)}) \quad (18)$$

where $f(\cdot, \cdot)$ denotes a base error function such as the MAE.

Note that in our definitions and notations, $\hat{Y}_f^{(n)} = \{\hat{y}_1^{(n)}, \hat{y}_2^{(n)}, \dots, \hat{y}_{t_n}^{(n)}\}$. We can therefore expand the total loss into a point-wise sum over all timesteps:

$$Loss = \sum_{n=1}^N \sum_{t=1}^{t_n} \lambda(n) * f(\hat{y}_t^{(n)}, x_t) \quad (19)$$

The underlying structure of this composite loss, visualized in Figure 10, reveals a key insight: BDO is not just a recursive forecasting process, but also a method for implicitly constructing a complex and adaptive structural loss. The properties of this loss can be finely tuned through several mechanisms: the stage-wise weighting coefficients, the forecast splitting strategy, the choice of the base error function, and even the architecture of each sub-forecaster.

E SUPPLEMENTARY RESULT

In addition to the results from hyperparameter searching, we also present a comparison under another common benchmark configuration: a fixed 96-length look-back window with unified hyperparameters for all prediction horizons. It is important to note, however, that this short-input setting inherently degrades the benefits of our BDO framework. Therefore, to isolate and highlight the effect of our proposals under these constraints, we make minimal adjustments to our best-performing model configuration. We retain most hyperparameters from our main experiments, adjusting only essential parameters like the number of layers for the 720-predict. Under this setup, we compare ReNF against the most recent state-of-the-art models, including OLinear, TQNet, TimeBridge, and CARD.

As shown in Table 6, ReNF remains highly competitive against the most recent SOTA models. However, its performance advantage is less pronounced in this setting, particularly in terms of MAE. We hypothesize that when restricted to shorter look-back windows, the initial short-term forecasts in the BDO process are less accurate. Consequently, concatenating these noisier predictions can introduce disruptions that limit the full benefit of our paradigm. From another perspective, while our proposed methods are universally applicable, these results also highlight the value of more specialized techniques in further enhancing the capabilities of Neural Forecasters.

E.1 MORE ABLATIONS

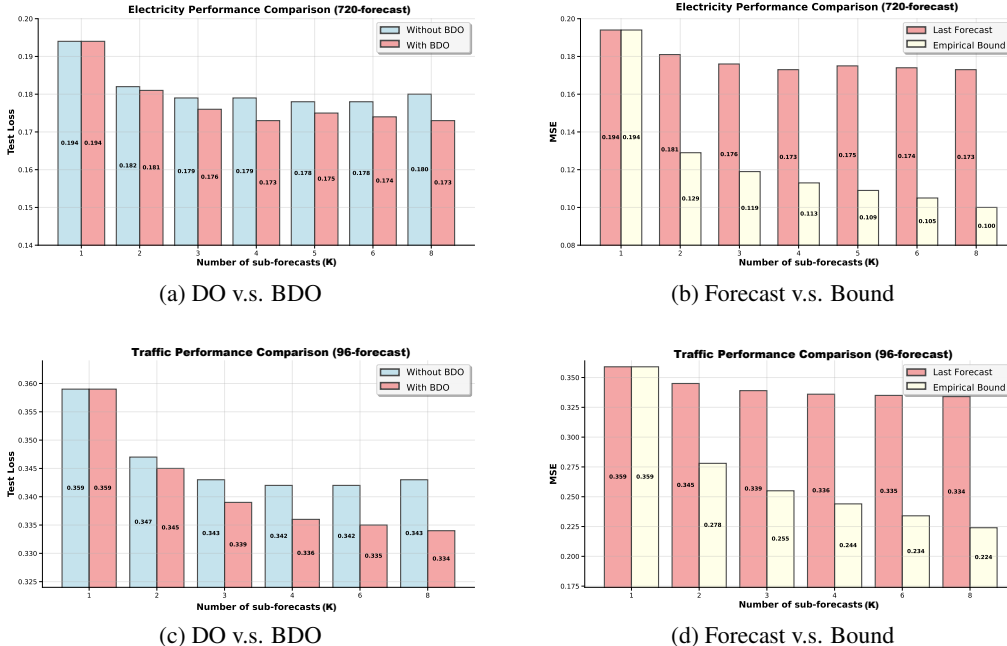


Figure 11: Supplementary illustrations of the performance variation with different numbers of sub-forecasts K. (a). Comparison of using DO or BDO with the Electricity dataset. (b). Comparison between the best forecast and the empirical bound of ReNF with the Electricity dataset. (c). Comparison of using DO or BDO with the Traffic dataset. (d). Comparison between the best forecast and the empirical bound of ReNF with the Traffic dataset.

EMA Smoothing. The results in Table 8 confirm that EMA smoothing yields substantial improvements in final forecast accuracy. This empirically validates our hypothesis from Section 2: EMA

Models	Re-Bound		ReNF		TimeBridge		OLinear		TQNet		CARD		
	MSE	MAE	MSE	MAE	MSE	MAE	MSE	MAE	MSE	MAE	MSE	MAE	
Weather	96	0.119	0.161	0.159	0.198	0.171	0.207	<u>0.153</u>	<u>0.190</u>	0.157	0.200	0.150	0.188
	192	0.151	0.197	0.206	0.242	0.220	0.250	0.200	0.235	0.206	0.245	<u>0.202</u>	<u>0.238</u>
	336	0.188	0.227	0.261	0.284	0.274	0.290	0.258	0.280	0.262	0.287	<u>0.260</u>	<u>0.282</u>
	720	0.219	0.249	<u>0.341</u>	<u>0.337</u>	0.352	0.341	0.337	0.333	0.344	0.342	0.343	0.353
	Avg.	0.165	0.203	0.242	0.265	0.254	0.272	0.237	0.260	0.242	0.269	<u>0.239</u>	0.265
Electricity	96	0.087	0.173	0.130	0.220	0.139	0.232	<u>0.131</u>	<u>0.221</u>	0.134	0.229	0.141	0.233
	192	0.098	0.186	0.146	0.235	0.158	0.250	<u>0.150</u>	<u>0.238</u>	0.154	0.247	0.160	0.250
	336	0.106	0.197	0.158	0.249	0.179	0.270	<u>0.165</u>	<u>0.254</u>	0.169	0.264	0.173	0.263
	720	0.117	0.209	0.182	0.274	0.208	0.296	<u>0.191</u>	<u>0.279</u>	0.201	0.294	0.197	0.284
	Avg.	0.102	0.191	0.154	0.245	0.171	0.262	<u>0.159</u>	<u>0.248</u>	0.165	0.259	0.168	0.258
Traffic	96	0.280	0.176	0.375	<u>0.238</u>	<u>0.386</u>	0.248	0.398	0.226	0.413	0.261	0.419	0.269
	192	0.287	0.184	0.398	<u>0.250</u>	<u>0.404</u>	0.257	0.439	0.241	0.432	0.271	0.443	0.276
	336	0.298	0.191	0.412	<u>0.257</u>	<u>0.415</u>	0.264	0.464	0.250	0.450	0.277	0.460	0.283
	720	0.330	0.208	0.444	<u>0.277</u>	<u>0.456</u>	0.286	0.502	0.270	0.486	0.295	0.490	0.299
	Avg.	0.299	0.190	0.407	<u>0.256</u>	<u>0.415</u>	0.264	0.451	0.247	0.445	0.276	0.453	0.282
Solar	96	0.090	0.139	0.173	<u>0.198</u>	0.190	0.208	0.180	0.191	<u>0.173</u>	0.233	0.197	0.211
	192	0.106	0.155	<u>0.206</u>	<u>0.225</u>	0.223	0.231	0.209	0.213	0.199	0.257	0.234	0.234
	336	0.119	0.170	<u>0.224</u>	<u>0.246</u>	0.242	0.250	0.231	0.229	0.211	0.263	0.256	0.250
	720	0.120	0.174	<u>0.231</u>	<u>0.256</u>	0.249	0.256	0.241	0.236	0.209	0.270	0.260	0.254
	Avg.	0.109	0.160	0.209	0.231	0.226	0.236	0.215	0.217	0.198	0.256	0.237	0.237
ETTh1	96	0.215	0.273	0.298	0.332	0.313	0.345	<u>0.302</u>	<u>0.334</u>	0.311	0.353	0.316	0.347
	192	0.252	0.295	0.350	0.361	0.367	0.378	0.357	<u>0.363</u>	<u>0.356</u>	0.378	0.363	0.370
	336	0.277	0.313	0.380	0.385	0.396	0.399	<u>0.387</u>	<u>0.385</u>	0.390	0.401	0.392	0.390
	720	0.321	0.340	0.436	0.425	0.457	0.440	<u>0.452</u>	<u>0.426</u>	0.452	0.440	0.458	0.425
	Avg.	0.266	0.305	0.366	0.376	0.383	0.391	<u>0.373</u>	<u>0.377</u>	0.377	0.393	0.382	0.383
ETTh2	96	0.138	0.219	0.168	0.246	0.174	0.251	<u>0.169</u>	0.249	0.173	0.256	0.169	<u>0.248</u>
	192	0.185	0.254	0.232	0.290	0.242	0.297	<u>0.232</u>	<u>0.290</u>	0.238	0.298	0.234	0.292
	336	0.230	0.285	0.289	0.328	0.302	0.338	<u>0.291</u>	<u>0.328</u>	0.301	0.340	0.294	0.339
	720	0.299	0.328	0.384	0.385	0.408	0.398	<u>0.389</u>	<u>0.387</u>	0.397	0.396	0.390	0.388
	Avg.	0.213	0.272	0.268	0.312	0.282	0.321	<u>0.269</u>	<u>0.314</u>	0.277	0.323	0.272	0.317
ETTh1	96	0.253	0.305	0.360	<u>0.383</u>	0.377	0.392	<u>0.360</u>	0.382	0.371	0.393	0.383	0.391
	192	0.288	0.328	0.410	0.414	0.429	0.421	<u>0.416</u>	<u>0.414</u>	0.428	0.426	0.435	0.420
	336	0.321	0.347	0.448	0.435	0.470	0.443	<u>0.457</u>	<u>0.438</u>	0.476	0.446	0.479	0.442
	720	0.292	0.342	0.442	0.454	0.477	0.473	<u>0.463</u>	<u>0.462</u>	0.487	0.470	0.471	0.461
	Avg.	0.289	0.331	0.415	0.422	0.438	0.432	<u>0.424</u>	<u>0.424</u>	0.441	0.434	0.442	0.429
ETTh2	96	0.227	0.286	0.281	<u>0.331</u>	0.287	0.334	0.284	0.329	0.295	0.343	<u>0.282</u>	0.331
	192	0.291	0.327	0.359	0.379	0.362	0.383	<u>0.360</u>	<u>0.379</u>	0.367	0.393	0.363	0.381
	336	0.323	0.354	0.398	0.412	0.417	0.425	<u>0.409</u>	<u>0.415</u>	0.417	0.427	0.411	0.418
	720	0.297	0.349	0.407	0.429	0.436	0.448	<u>0.415</u>	<u>0.431</u>	0.433	0.446	0.416	0.431
	Avg.	0.285	0.329	0.361	0.388	0.376	0.398	<u>0.367</u>	<u>0.389</u>	0.378	0.402	0.368	0.390

Table 6: Full results of long-term forecasting of unified hyperparameter. The Re-Bound column denotes the empirical bound discussed in Sec.3.3. The look-back window is fixed to 96 for all baselines. All results are averaged across four different prediction lengths. The best and second-best results are highlighted in red and blue, respectively.

mitigates the detrimental effects of flawed early stopping, where volatile validation scores lead to the premature saving of suboptimal models. By providing a more reliable and stable training signal, EMA not only enhances performance but also establishes the robust foundation necessary to fairly evaluate our other contributions, such as the BDO paradigm.

Models	Re-Bound		ReNF		TimeBridge		DUET		TimeDistill		Timer-XL		iTransformer		TimeMixer		PatchTST		Crossformer		DLiner		
	MSE	MAE	MSE	MAE	MSE	MAE	MSE	MAE	MSE	MAE	MSE	MAE	MSE	MAE	MSE	MAE	MSE	MAE	MSE	MAE	MSE	MAE	
Weather	96	0.110	0.149	0.138	0.180	<u>0.144</u>	<u>0.184</u>	0.146	0.191	0.145	0.204	0.157	0.205	0.157	0.206	0.147	0.198	0.150	0.200	0.143	0.210	0.170	0.230
	192	0.141	0.185	0.182	0.224	<u>0.186</u>	<u>0.226</u>	0.188	0.231	0.188	0.247	0.206	0.250	0.200	0.248	0.192	0.242	0.191	0.239	0.195	0.261	0.216	0.273
	336	0.177	0.216	0.231	0.266	<u>0.237</u>	<u>0.267</u>	<u>0.235</u>	0.269	0.240	0.286	0.259	0.291	0.252	0.287	0.247	0.284	0.242	0.279	0.254	0.319	258	0.307
	720	0.232	0.261	0.304	0.318	0.312	<u>0.321</u>	<u>0.308</u>	<u>0.319</u>	0.310	0.338	0.337	0.344	0.320	0.336	0.318	0.330	0.312	0.330	0.335	0.385	0.323	0.362
	Avg.	0.165	0.203	0.214	0.247	0.220	<u>0.250</u>	<u>0.219</u>	0.253	0.221	0.269	0.240	0.273	0.232	0.269	0.226	0.264	0.224	0.262	0.232	0.294	0.242	0.293
Electricity	96	0.083	0.171	0.118	0.210	<u>0.122</u>	<u>0.216</u>	0.128	0.219	0.128	0.225	0.127	0.219	0.134	0.230	0.153	0.256	0.143	0.247	0.134	0.231	0.140	0.237
	192	0.097	0.186	0.138	0.229	<u>0.143</u>	0.238	0.145	<u>0.235</u>	0.145	0.241	0.145	0.236	0.154	0.250	0.168	0.269	0.158	0.261	0.146	0.243	0.154	0.251
	336	0.105	0.196	0.151	0.244	<u>0.163</u>	0.258	0.163	<u>0.255</u>	0.161	0.258	0.159	0.252	0.169	0.265	0.189	0.291	0.168	0.267	0.165	0.264	0.169	0.268
	720	0.115	0.207	0.173	0.266	<u>0.178</u>	<u>0.274</u>	0.193	0.281	0.195	0.291	0.187	0.277	0.194	0.288	0.228	0.320	0.214	0.307	0.237	0.314	0.204	0.301
	Avg.	0.100	0.190	0.145	0.237	<u>0.152</u>	<u>0.247</u>	0.157	0.248	0.157	0.254	0.155	0.246	0.163	0.258	0.185	0.284	0.171	0.271	0.171	0.263	0.167	0.264
Traffic	96	0.234	0.167	<u>0.335</u>	0.226	<u>0.332</u>	<u>0.237</u>	0.360	0.238	0.358	0.256	0.340	0.238	0.358	0.258	0.369	0.257	0.370	0.262	0.526	0.288	0.395	0.275
	192	0.245	0.175	<u>0.356</u>	0.239	0.343	0.239	0.383	0.249	0.374	0.264	0.360	0.248	0.382	0.271	0.399	0.272	0.386	0.269	0.503	0.263	0.407	0.280
	336	0.254	0.180	<u>0.366</u>	0.246	0.360	0.249	0.395	0.259	0.389	0.271	0.377	0.256	0.396	0.277	0.407	0.272	0.396	0.275	0.505	0.276	0.417	0.286
	720	0.284	0.197	<u>0.402</u>	0.267	0.392	0.268	0.435	0.278	0.428	0.292	0.418	0.279	0.445	0.308	0.461	0.316	0.435	0.295	0.552	0.301	0.454	0.308
	Avg.	0.254	0.180	<u>0.365</u>	0.245	<u>0.357</u>	<u>0.248</u>	0.393	0.256	0.387	0.271	0.374	0.255	0.395	0.279	0.409	0.279	0.397	0.275	0.522	0.282	0.418	0.287
Solar	96	0.082	0.141	0.157	0.202	<u>0.159</u>	0.196	0.166	0.211	0.166	0.229	0.162	0.221	0.190	0.244	0.179	0.232	0.170	0.234	0.183	0.208	0.199	0.265
	192	0.087	0.145	0.174	0.210	0.173	0.215	0.199	0.212	0.181	0.239	0.187	0.239	0.193	0.257	0.201	0.259	0.204	0.302	0.208	0.227	0.220	0.281
	336	0.099	0.156	0.180	0.219	0.193	0.229	0.207	0.215	<u>0.191</u>	0.246	0.205	0.255	0.203	0.266	0.190	0.256	0.212	0.293	0.212	0.239	0.234	0.295
	720	0.092	0.151	0.190	0.225	<u>0.207</u>	<u>0.237</u>	0.206	0.217	0.199	0.252	0.238	0.279	0.223	0.281	0.203	0.261	0.215	0.307	0.215	0.256	0.243	0.301
	Avg.	0.090	0.148	0.176	0.214	<u>0.183</u>	0.219	0.195	<u>0.214</u>	0.184	0.242	0.198	0.249	0.202	0.262	0.193	0.252	0.200	0.284	0.205	0.233	0.224	0.286
ETTh1	96	0.189	0.262	0.270	0.325	0.288	0.339	<u>0.279</u>	<u>0.333</u>	0.285	0.344	0.290	0.341	0.300	0.353	0.293	0.345	0.289	0.342	0.314	0.367	0.300	0.345
	192	0.218	0.284	0.310	0.352	0.326	0.368	<u>0.320</u>	<u>0.358</u>	0.331	0.368	0.337	0.369	0.341	0.380	0.335	0.372	0.329	0.368	0.374	0.410	0.336	0.366
	336	0.242	0.300	0.343	0.373	0.363	0.394	<u>0.348</u>	<u>0.377</u>	0.359	0.386	0.374	0.393	0.374	0.396	0.368	0.386	0.362	0.390	0.413	0.432	0.367	0.387
	720	0.249	0.296	0.400	0.405	0.417	0.419	<u>0.405</u>	<u>0.408</u>	0.415	0.416	0.437	0.428	0.429	0.430	0.426	0.417	0.416	0.423	0.416	0.423	0.375	0.417
	Avg.	0.225	0.286	0.331	0.364	0.349	0.380	<u>0.338</u>	<u>0.369</u>	0.348	0.380	0.359	0.382	0.361	0.390	0.356	0.380	0.349	0.381	0.464	0.456	0.356	0.379
ETTh2	96	0.131	0.214	0.157	0.241	<u>0.157</u>	<u>0.243</u>	0.162	0.249	0.163	0.255	0.175	0.257	0.175	0.266	0.165	0.256	0.165	0.255	0.296	0.391	0.164	0.256
	192	0.174	0.246	0.212	0.279	0.218	<u>0.284</u>	<u>0.215</u>	0.288	0.220	0.294	0.242	0.301	0.242	0.312	0.225	0.298	0.221	0.293	0.369	0.416	0.224	0.304
	336	0.216	0.276	0.262	0.315	0.270	<u>0.321</u>	<u>0.267</u>	0.321	0.269	0.328	0.293	0.337	0.282	0.337	0.277	0.332	0.276	0.327	0.588	0.600	0.277	0.337
	720	0.283	0.322	0.341	0.368	<u>0.344</u>	0.372	0.348	0.373	0.346	<u>0.369</u>	0.376	0.390	0.375	0.394	0.360	0.385	0.362	0.381	0.750	0.612	0.371	0.401
	Avg.	0.201	0.265	0.243	0.301	<u>0.247</u>	<u>0.305</u>	0.248	0.308	0.250	0.312	0.271	0.322	0.269	0.327	0.257	0.318	0.256	0.314	0.501	0.505	0.259	0.325
ETTh1	96	0.243	0.300	0.350	0.383	0.355	0.391	<u>0.353</u>	<u>0.386</u>	0.373	0.401	0.364	0.397	0.386	0.405	0.372	0.401	0.377	0.397	0.411	0.435	0.379	0.403
	192	0.276	0.327	0.385	0.408	<u>0.389</u>	0.414	0.398	<u>0.409</u>	0.411	0.426	0.405	0.424	0.424	0.440	0.413	0.429	0.409	0.425	0.409	0.438	0.408	0.419
	336	0.294	0.342	0.405	0.425	<u>0.415</u>	0.435	0.415	<u>0.428</u>	0.439	0.444	0.427	0.439	0.449	0.460	0.438	0.450	0.431	0.444	0.433	0.457	0.440	0.440
	720	0.266	0.322	0.422	0.449	<u>0.443</u>	0.462	0.436	<u>0.458</u>	0.495	0.493	0.439	0.459	0.495	0.487	0.486	0.484	0.457	0.477	0.501	0.514	0.471	0.493
	Avg.	0.270	0.323	0.391	0.416	<u>0.401</u>	0.426	0.401	<u>0.420</u>	0.430	0.441	0.409	0.430	0.439	0.448	0.427	0.441	0.419	0.436	0.439	0.461	0.425	0.439
ETTh2	96	0.214	0.285	0.261	0.329	<u>0.270</u>	<u>0.331</u>	0.271	0.335	0.273	0.336	0.277	0.343	0.297	0.348	0.281	0.351	0.274	0.337	0.728	0.603	0.300	0.364
	192	0.261	0.320	0.320	0.370	0.338	<u>0.375</u>	<u>0.335</u>	0.376	0.334	0.381	0.348	0.391	0.372	0.403	349	0.387	0.348	0.384	0.723	0.607	0.387	0.423
	336	0.270	0.327	0.346	0.394	0.370	0.402	<u>0.354</u>	<u>0.398</u>	0.363	0.415	0.375	0.418	0.388	0.418	0.366	0.413	0.377	0.416	0.740	0.628	0.490	0.487
	720	0.261	0.325	0.381	0.423	0.402	0.434	<u>0.384</u>	<u>0.426</u>	0.408	0.446	0.409	0.458	0.424	0.444	0.401	0.436	0.406	0.441	1.386	0.882	0.704	0.597
	Avg.	0.252	0.314	0.327	0.379	0.345	0.386	<u>0.336</u>	<u>0.384</u>	0.345	0.395	0.352	0.402	0.370	0.403	0.349	0.397	0.351	0.395	0.894	0.680	0.470	0.468

Table 7: Full results of long-term forecasting of hyperparameter searching. The Re-Bound column denotes the empirical bound discussed in Sec.3.3. The look-back window is searched from {336, 512, 720} for the best performance. Timer-XL uses a 672-length window as the original paper. All results are averaged across four different prediction lengths: {96, 192, 336, 720}. The best and second-best results are highlighted in red and blue, respectively.

Pre-Dropout. Our MLP architecture applies dropout to the input data by default as a regularization technique. While its impact can be subtle and dataset-dependent, we perform an ablation study for the sake of completeness. The results of this analysis on the ETTh1, ETTh2, and Electricity datasets are presented in Table 10.

E.2 ROUBUSTENESS

In Table 9, we present the error bar of ReNF in datasets with relatively small sizes or high instability. It shows that ReNF exhibits high robustness because of its simple structure, which is a favorable characteristic for industrial applications.

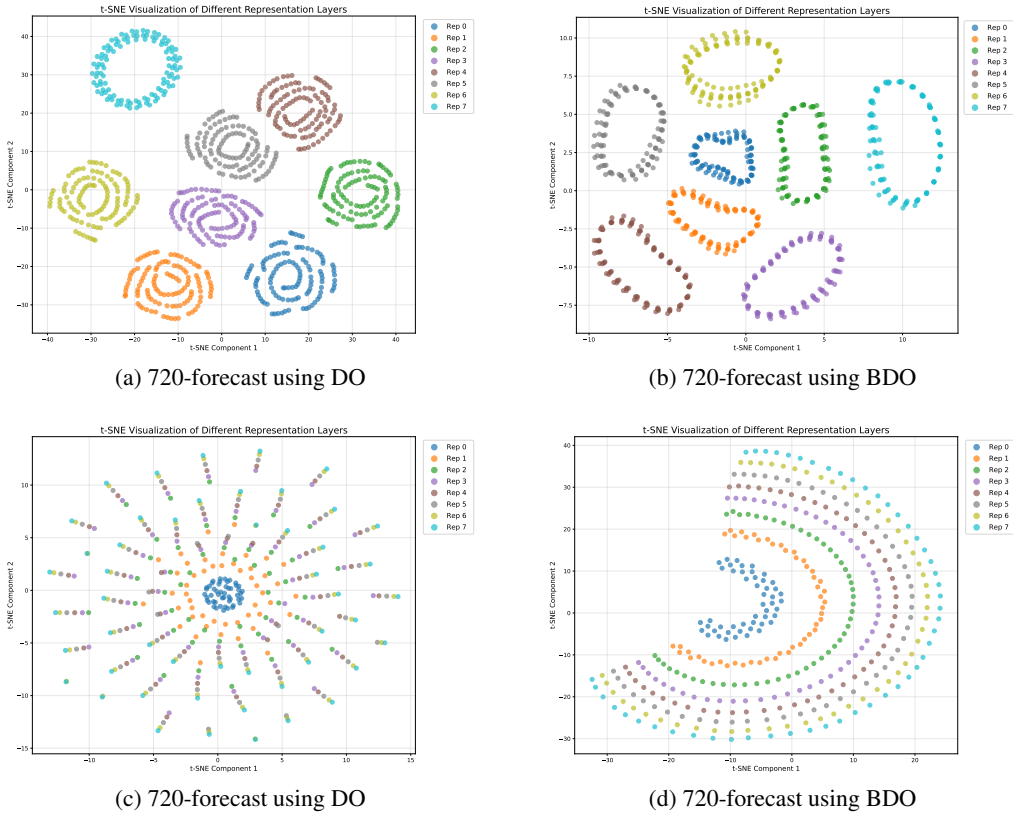


Figure 12: Visualizations of the representations of different layers/sub-forecasters. (a). representations of using DO with the ETTh1 dataset. (b). representations of using BDO with the ETTh1 dataset. (c). representations of using DO with the ETTm1 dataset. (d). representations of using BDO with the ETTm1 dataset.

E.3 FURTHER EXPLORATIONS

Two Factors of BDO. We wish to clarify that our BDO paradigm is comprised of two distinct and essential mechanisms. The first is the addition of a linear head to each block, which generates an explicit sub-forecast from the intermediate representation. The second is the recursive concatenation of this sub-forecast with the input for the subsequent stage, which encourages the network to implicitly learn a post-combination function as motivated by MNFT. To disentangle their respective contributions, we conduct an ablation study on these two factors.

The results on the Electricity, ETTh1, and ETTm1 datasets, shown in Table 11, indicate that the two components are synergistic; removing either one leads to a notable degradation in performance. Overall, we find that the hierarchical supervision from the sub-forecasts plays a more significant role. This is expected, as it not only allows for repeated reuse of label information but also enforces a causal and homogeneous structure on the predictive representations across layers, an effect we visualize in Figure 12. However, a few anomalous results suggest that other unresolved factors, such as the quality of the ground truth labels, may also influence performance in certain cases.

Preference of Deep Representations. In Sec. 2.4, we introduce two variants of MLPs with a few differences. The primary distinction is the inclusion of skip-connections between representations in ReNF- β , which facilitates the learning of deeper, more complex non-linear dynamics. To justify this design choice, the following experiments demonstrate the performance degradation that occurs when a model’s complexity is mismatched with the dataset’s intrinsic characteristics.

Specifically, we apply the ReNF- β to the ETTh1 and ETTh2 datasets, and apply the alpha version to the large volume Electricity and Traffic datasets. The results are shown in the Table 12, from which

Variants		ReNF		ReNF	
		origin		w/o EMA	
Metric		MSE	MAE	MSE	MAE
ETTh1	96	0.350	0.383	0.357	0.387
	192	0.385	0.408	0.407	0.421
	336	0.405	0.425	0.426	0.435
	720	0.422	0.449	0.447	0.467
	Avg.	0.391	0.416	0.409	0.428
ETTh2	96	0.261	0.329	0.265	0.329
	192	0.320	0.370	0.336	0.375
	336	0.346	0.394	0.397	0.418
	720	0.381	0.423	0.421	0.441
	Avg.	0.327	0.379	0.355	0.391
ETTm1	96	0.270	0.325	0.303	0.347
	192	0.310	0.352	0.341	0.371
	336	0.343	0.373	0.362	0.386
	720	0.401	0.406	0.425	0.420
	Avg.	0.331	0.364	0.358	0.381
ETTm2	96	0.157	0.241	0.162	0.246
	192	0.212	0.279	0.221	0.285
	336	0.262	0.315	0.272	0.322
	720	0.341	0.368	0.352	0.374
	Avg.	0.243	0.301	0.252	0.307

Variants		ReNF		ReNF	
		origin		w/o EMA	
Metric		MSE	MAE	MSE	MAE
Weather	96	0.138	0.180	0.139	0.182
	192	0.181	0.224	0.184	0.227
	336	0.231	0.266	0.232	0.266
	720	0.304	0.318	0.308	0.320
	Avg.	0.214	0.247	0.216	0.249
Electricity	96	0.118	0.210	0.124	0.218
	192	0.138	0.229	0.145	0.239
	336	0.151	0.244	0.156	0.252
	720	0.173	0.266	0.182	0.277
	Avg.	0.145	0.237	0.152	0.247
Traffic	96	0.335	0.226	0.341	0.237
	192	0.356	0.239	0.363	0.249
	336	0.366	0.246	0.373	0.256
	720	0.402	0.267	0.411	0.278
	Avg.	0.365	0.245	0.372	0.255
Solar	96	0.157	0.202	0.177	0.232
	192	0.174	0.210	0.193	0.234
	336	0.180	0.219	0.195	0.239
	720	0.190	0.225	0.199	0.242
	Avg.	0.176	0.214	0.191	0.237

Table 8: Full numerical results on the effect of EMA smoothing.

Model	ReNF		TimeBridge		Confidence
	MSE	MAE	MSE	MAE	
Dataset					Interval
ETTh1	0.391 ± 0.000	0.417 ± 0.000	0.399 ± 0.009	0.424 ± 0.008	99%
ETTh2	0.327 ± 0.000	0.380 ± 0.000	0.343 ± 0.018	0.383 ± 0.014	99%
Weather	0.214 ± 0.000	0.247 ± 0.000	0.219 ± 0.006	0.250 ± 0.003	99%
Solar	0.177 ± 0.000	0.215 ± 0.000	0.182 ± 0.003	0.219 ± 0.003	99%

Table 9: Standard deviation and statistical tests for ReNF and TimeBridge on ETTh1, ETTh2, Weather, and Solar datasets. The results are based on the average performance across four prediction lengths from five runs with different random seeds.

we can deduce that the complex deep representations of ReNF- β are clearly detrimental to ETTh datasets. In stark contrast, large-volume datasets like Electricity and Traffic benefit from deeper, more expressive representations. This finding provides a direct explanation, from the perspective of representation depth, for the recurring phenomenon where simpler, parsimonious NFs outperform more complex ones on certain benchmarks. It underscores the critical importance of matching model capacity to the intrinsic characteristics of the time series data, identifying a clear direction for future work in adaptive forecaster design.

F LIMITATION AND FURTHER DISCUSSION

The Multiple Neural Forecasting Theorem (MNFT) presented in this paper is foundational but preliminary. While it provides the core intuition for our work, a more rigorous and deeper exploration of its theoretical properties or deriving other related theorems could inspire new and promising research directions.

Variants		ReNF		ReNF	
		origin		w/o pre-drop	
Metric		MSE	MAE	MSE	MAE
ETTh1	96	0.350	0.383	0.352	0.386
	192	0.385	0.408	0.385	0.410
	336	0.405	0.425	0.406	0.429
	720	0.422	0.449	0.428	0.454
	Avg.	0.391	0.416	0.393	0.420
ETTh2	96	0.261	0.329	0.260	0.329
	192	0.320	0.370	0.321	0.370
	336	0.346	0.394	0.348	0.396
	720	0.381	0.423	0.383	0.425
	Avg.	0.327	0.379	0.328	0.380
Electricity	96	0.118	0.210	0.119	0.210
	192	0.138	0.229	0.138	0.229
	336	0.151	0.244	0.150	0.243
	720	0.173	0.266	0.175	0.267
	Avg.	0.145	0.237	0.146	0.237

Table 10: Effects of pre-drop on selected datasets.

Variants		ReNF		ReNF		ReNF	
		origin		w/o factor_1		w/o factor_2	
Metric		MSE	MAE	MSE	MAE	MSE	MAE
Electricity	96	0.118	0.210	0.119	0.211	0.123	0.215
	192	0.138	0.229	0.138	0.229	0.145	0.236
	336	0.151	0.244	0.153	0.245	0.156	0.251
	720	0.173	0.266	0.179	0.271	0.177	0.269
	Avg.	0.145	0.237	0.147	0.239	0.150	0.243
ETTh1	96	0.350	0.383	0.356	0.382	0.356	0.382
	192	0.385	0.408	0.394	0.406	0.394	0.407
	336	0.405	0.427	0.420	0.427	0.420	0.425
	720	0.422	0.449	0.432	0.454	0.436	0.456
	Avg.	0.391	0.417	0.400	0.417	0.402	0.418
ETTh2	96	0.270	0.325	0.273	0.327	0.275	0.327
	192	0.310	0.352	0.311	0.355	0.312	0.353
	336	0.343	0.373	0.343	0.376	0.342	0.374
	720	0.401	0.406	0.398	0.409	0.413	0.410
	Avg.	0.331	0.364	0.331	0.367	0.336	0.366
Solar	96	0.157	0.202	0.165	0.201	0.170	0.217
	192	0.174	0.210	0.185	0.215	0.195	0.226
	336	0.180	0.219	0.185	0.219	0.189	0.233
	720	0.190	0.225	0.197	0.227	0.197	0.238
	Avg.	0.176	0.214	0.183	0.216	0.188	0.229

Table 11: Ablations on the two factors of our BDO implementation. The factor_1 denotes the concatenation in input space, and factor_2 denotes the computation of the sub-forecasting losses.

Specifically, under the paradigm of MNFT, the role of Neural Network (NN) in this area becomes transparent. First and perhaps most importantly, we should leverage NN’s capability to create a powerful post-combination function. While our BDO paradigm is effective, the current recursive strategy for combining sub-forecasts is not fully optimal. This is evident from the performance gap between our final forecast and the theoretical empirical bound as the number of stages increases.

Variants		ReNF		ReNF	
		origin		exchange	
Metric		MSE	MAE	MSE	MAE
ETTh1	96	0.350	0.383	0.384	0.410
	192	0.385	0.408	0.407	0.428
	336	0.405	0.425	0.447	0.456
	720	0.422	0.449	0.502	0.493
	Avg.	0.391	0.416	0.435	0.447
ETTh2	96	0.261	0.329	0.271	0.332
	192	0.320	0.370	0.340	0.376
	336	0.346	0.394	0.381	0.410
	720	0.381	0.423	0.415	0.437
	Avg.	0.327	0.379	0.352	0.389
Electricity	96	0.118	0.210	0.125	0.217
	192	0.138	0.229	0.144	0.235
	336	0.151	0.244	0.160	0.252
	720	0.173	0.266	0.196	0.283
	Avg.	0.145	0.237	0.156	0.247
Traffic	96	0.335	0.226	0.359	0.241
	192	0.356	0.239	0.377	0.249
	336	0.366	0.246	0.389	0.259
	720	0.402	0.267	0.426	0.284
	Avg.	0.365	0.245	0.388	0.258

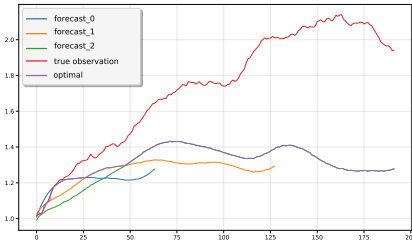
Table 12: Performances degrade drastically after using NFs with an improper degree of complexity. The Exchange column denotes that the version of ReNF (α and β) is alternated.

Developing more intricate methods to better leverage the full set of sub-forecasts could lead to substantial accuracy gains. Furthermore, the benefit of BDO is less pronounced on certain datasets, such as ETTm2. The underlying reasons for this variance warrant further investigation.

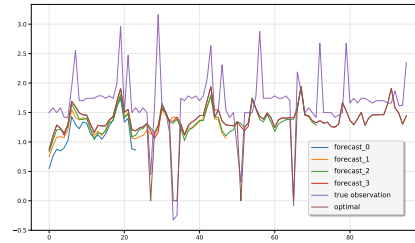
Second, we are consistently supposed to build more powerful Neural Forecasting Machines (NFM) to approximate the expected distributions of future data, thereby reducing the bias b in the MNFT C. Therefore, a comprehensive study is needed to verify the effects of our proposed techniques when applied to other advanced model architectures beyond MLPs.

Finally, this work develops the BDO paradigm specifically for the LTSF setting. A key open question is how this paradigm can be adapted for short-term forecasting tasks, which could ultimately lead to a more unified framework for time series forecasting.

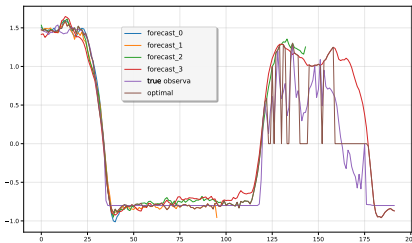
G VISUALIZATION OF PREDICTION



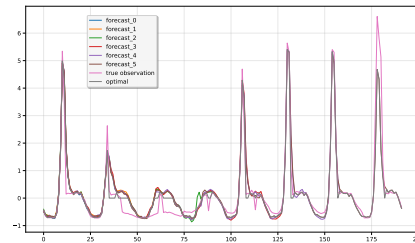
(a) 192-prediction on the weather dataset



(b) 192-prediction on the Electricity dataset

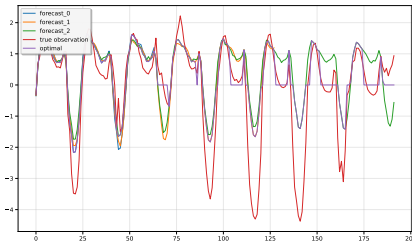


(c) 192-prediction on the Solar dataset

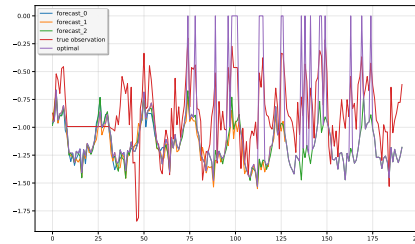


(d) 192-prediction on the Traffic dataset

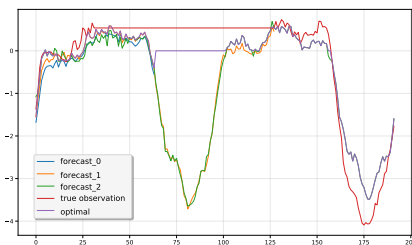
Figure 13: Full visualization of forecasting results of ReNF. The figure shows multiple outputs of ReNF in different layers, along with the result of applying optimal post-combination.



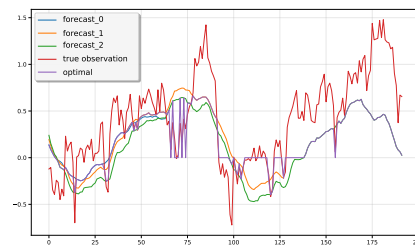
(a) 192-prediction on the ETTh1 dataset



(b) 192-prediction on the ETTh2 dataset



(c) 192-prediction on the ETTm1 dataset



(d) 192-prediction on the ETTm2 dataset

Figure 14: Full visualization of forecasting results of ReNF. The figure shows multiple outputs of ReNF in different layers, along with the result of applying optimal post-combination.

H DECLARATION OF THE LLMs USE

We utilized a Large Language Model (LLM) to assist in refining the language of this manuscript. The LLM was used specifically to check for grammatical correctness and to improve the clarity and flow of expressions, ensuring a professional academic tone. The sole purpose of using the LLM was to enhance the readability and comprehensibility of the paper based on our first draft. All other contents, including the core ideas, presentation logic, experimental design, and results, are entirely our own.